Nanosecond Temperature Jump and Time-Resolved Raman Study of Thermal Unfolding of Ribonuclease A

Kohji Yamamoto,* Yasuhisa Mizutani,*† and Teizo Kitagawa*†
*School of Mathematical and Physical Science, The Graduate University for Advanced Studies and †Institute for Molecular Science, Okazaki National Research Institutes, Myodaiji, Okazaki 444-8585, Japan

ABSTRACT A nanosecond temperature jump (T-jump) apparatus was constructed and combined with time-resolved Raman measurements to investigate thermal unfolding of a protein for the first time. The 1.56-μm heat pulse with 9 ns width at 10 Hz was obtained through the two-step stimulated Raman scattering in D_2 gas involving seeding and amplification. To achieve uniform temperature rise, the counter-propagation geometry was adopted for the heat pulse. The temperature rise was determined by anti-Stokes to Stokes intensity ratios of the 317 and 897 cm^{-1} bands of MoO_4^{2-} ions in an aqueous solution. The T-jump as large as 9°C in 10 ns was attained. The unfolding of bovine pancreatic ribonuclease A was monitored with time-resolved Raman spectra excited at 532 nm. The C-S stretching band of Met residues exhibited 10% change of that expected from the stationary state temperature-difference spectra in the initial 200 ns following T-jump and another 10% in 5 ms. The Raman intensity of SO_4^{2-} ions around 980 cm^{-1} increased at 100 μs, presumably due to some conformational changes of the protein around the active site. The S–S stretches and tyrosine doublet displayed little changes within 5 ms. Thus, the conformational changes in the initial step of unfolding are not always concerted.

INTRODUCTION

Elucidation of protein folding mechanism is becoming a current topic of fast time-resolved spectroscopy since Anfinsen (1973) found that the nature of interactions responsible for protein folding is determined solely by the amino acid sequence of the protein. The folding/unfolding kinetics of long polypeptides and model compounds were initially investigated using dielectric loss (Schwarz and Seelig, 1968), ultrasonic absorption (Burke et al., 1965; Schwarz, 1965; Parker et al., 1968; Hammes and Roberts, 1969; Barksdale and Stuehr, 1972; Wada et al., 1972), temperature jump (Sano et al., 1975), and electric-field jump (Cummings and Eyring, 1975; Tsuji et al., 1976), as summarized by Gruenewald et al. (1979). Recently, the temperature jump (T-jump) was revisited because of developments in modern laser techniques (Phillips et al., 1995; Ballew et al., 1996; Williams et al., 1996; Gilmanshin et al., 1997). Early attempts using dyes to absorb Q-switched pulses from ruby and glass lasers to provide radiation at 694 nm (Staerk and Czerlinski, 1965) and 1060 nm (Hoffman et al., 1968), respectively, succeeded in producing T-jump of ~4°C. Raman shifting of the Nd:YAG laser fundamental (1064 nm) by methane to 1.54 μm was used to heat water directly (Williams et al., 1989), whereas the difference mixing of a Nd:YAG laser-pumped two-dye laser outputs by $LiNbO_3$ crystal was used to generate longer wavelength pulses (2.0 μm, ~7 ns) (Gilmanshin et al., 1997).

The secondary structure formation of polypeptides has been pursued with fluorescence of tryptophan (Trp) or 4-(methylamino) benzoic acid (MABA) as a fast probe. Eaton and coworkers (1998) extensively applied the fluorescence probe in combination with the laser T-jump to explore the nucleation and growth of α-helix (Thompson et al., 1997) and β-hairpin (Munoz et al., 1997) of polypeptides. Gruebele and coworkers (Ballew et al., 1996; Gruebele et al., 1998) also monitored the Trp fluorescence intensities and lifetimes to study temperature-induced folding of cold-denatured apomyoglobin with 10-ns pulses at 1.54 μm. However, vibrational spectroscopy can provide more detailed information on hydrogen bonding of various side chains in addition to the secondary and tertiary structures of protein backbone (Harada and Takeuchi, 1986). Indeed, Dyer and coworkers (Williams et al., 1996; Gilmanshin et al., 1997) and Hochstrasser and coworkers (Phillips et al., 1995) investigated infrared spectra of proteins in combination with the laser T-jump, and Asher and coworkers (Lednev et al., 1999) applied UV resonance Raman spectroscopy to study a peptide. We succeeded in observing time-resolved nonresonant Raman spectra of a protein upon T-jump by a 9-ns near-infrared pulse for the first time (Yamamoto et al., 1999).

It is known that disulfide bonds play a critical role in the folding of many proteins and in the stabilization of native tertiary structures (Anfinsen and Scheraga, 1975). Bovine pancreatic ribonuclease A (RNase A) has been studied extensively to unravel its folding/unfolding pathways (Konishi et al., 1982; Wearne and Creighton, 1988; Rothwarf and Scheraga, 1993b; Li et al., 1995). RNase A is a 124-residue protein containing four native disulfide bonds (Cys-26–Cys-84, Cys-40–Cys-95, Cys-58–Cys-110, and Cys-65–Cys-72) as illustrated in Fig. 1 (Howlin et al., 1989). The folding pathway of RNase A might not be unique, and

Received for publication 1 November 1999 and in final form 30 March 2000.

Address reprint requests to Teizo Kitagawa at Institute for Molecular Science, Okazaki National Research Institutes, Myodaiji, Okazaki, 444-8585, Japan. Tel.: +81-564-55-7340; Fax: +81-564-55-4639; E-mail: teizo@ims.ac.jp.

0006-3495/00/07/485/11 $2.00

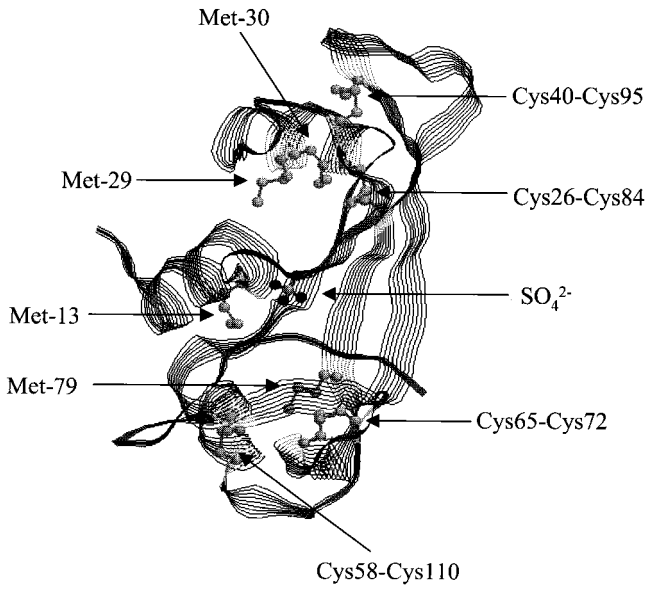

FIGURE 1 Structure of RNase A obtained by X-ray crystallography (Howlin et al., 1989). All the eight cysteine residues form four disulfide bridges; Cys-26–Cys-84, Cys-40–Cys-95, Cys-58–Cys-110, and Cys-65–Cys-72. All the disulfide bridges (C_α-$C_\beta H_2$-S_γ-S'_γ-$C'_\beta H_2$-C'_α) adopt the GGG conformation. The *trans* position of the sulfur atom in X-C[sub]α-$C_\beta H_2$-S_γ group is occupied by a carbon atom of an amide group in all the cysteine residues (P_C-form). Four methionine residues (Met-13, -29, -30, and -79) have two conformations regarding the X-C_β-$C_\gamma H_2$-S_δ-$C_\epsilon H_3$ group; one is the P_H-G form as seen for Met-13, -29, and -30 where hydrogen atom occupies the *trans* position of the sulfur atom with *gauche* form of C_β-$C_\gamma H_2$-S_δ-$C_\epsilon H_3$ and the other is the P_C-T form as seen for Met-79 where α-carbon occupies the *trans* position of the sulfur atom. A sulfate ion observed by X-ray crystallography is bound at the active site of RNase A.

the rate-determining steps in the major and minor populated pathways involve the formation of the three-disulfide species, which lacks the 40–95 or 65–72 bond (Li et al., 1995). Although the oxidative regeneration and reductive cleavage of the disulfide bond were suggested to be kinetically same (Li et al., 1995), the three-disulfide species lacking the 65–72 bond is thought to be the most highly populated intermediate in the unfolding pathways (Rothwarf and Scheraga, 1991). The role of the 65–72 bond was examined using des-[65–72]-RNase A, i.e., RNase A that lacks Cys-65–Cys-72 disulfide bond (Talluri et al., 1994), and it was found that the midpoint of the thermal transition of des-[65–72]-RNase A was 17.8°C lower than that of native RNase A, but that these two proteins have a close structural similarity in all regions with the only major differences in the loop region composed of residues 60–72. The recent ^1H, ^{15}N, and ^{13}C NMR studies revealed that the (C40A, C95A) mutant as well as wild-type proteins fold in a similar way (Laity et al., 1997). Thus, it is thought that the rate-determining step corresponds to a partial unfolding even in one region of the protein and not to a global conformational unfolding process. In contrast, relationships of the S–S stretching (ν_{SS}) (Sugeta et al., 1972, 1973; Sugeta, 1975) and C–S stretching (ν_{CS}) frequencies (Nogami et al., 1975a,b,c) with the dihedral angles of the C-C-S-S-C-C moiety have been investigated. Accordingly, we focused our attention on the side-chain conformational changes of RNase A upon T-jump by a nanosecond laser.

In the UV resonance Raman spectroscopy of proteins, Raman intensity is strong, and a small amount of dilute solution can give well-defined Raman signals, but the situation is quite different in the case of nonresonant Raman scattering. A relatively large amount of a concentrated protein solution is indispensable to get Raman signals, and this made it impossible to use the ordinary 1.89-μm pulse generated by H_2 Raman shift of a Q-switched Nd:YAG laser as a heat pulse. The reason for this is that the large absorption coefficient (61 cm^{-1}) of water at 1.89 μm limits the maximum thickness of the sample solution to 100 μm even with introduction of the counter-propagation geometry to achieve uniform heating. To utilize another absorption band of water with moderate absorbance, we searched other possibilities to obtain a heat pulse. A 1.54-μm pulse was generated by the CH_4 Raman shift of a Q-switched Nd:YAG laser, but CH_4 was not stable enough against a high repetition rate of excitation. In this study, we succeeded in generating a 1.56-μm pulse from the fundamental of the Q-switched Nd:YAG laser by the use of a Raman shift of D_2 gas. The performance of the T-jump apparatus with the 1.56-μm pulse, that was examined with the intensity ratio of anti-Stokes/Stokes bands of molybdate (MoO_4^{2-}) ions, will be explained first, and the results of its application to thermal unfolding of RNase A monitored by nanosecond time-resolved Raman spectroscopy follow it.

EXPERIMENTAL PROCEDURES

Sample preparation

RNase A (type IIIA, Sigma, St. Louis, MO) was purified by passage through two columns: first, ion exchange chromatography with sulphopropyl sepharose (SP Sepharose FF, Amersham Pharmacia Biotech, Uppsala, Sweden) equilibrated with 25 mM HEPES, 1 mM EDTA, pH 8.0 combined with linear gradient elution with 0–150 mM NaCl (Rothwarf and Scheraga, 1993a); and second, adsorption on an active carbon column activated with 1 M HCl. The passage through the second column removed the yellow color completely. Finally, the solvent was exchanged with 200 mM acetate buffer, pH 5.0 containing 40 mM Na_2SO_4, and the concentration of RNase A was adjusted to 7.0 mM on the basis of $\epsilon_M = 9.8 \times 10^3$ M^{-1} cm^{-1} at 278 nm (Sela and Anfinsen, 1957). The sample solution was degassed before putting it into the Raman cell to avoid generation of bubbles upon T-jump. This treatment practically reduced not only the stray light, and thus background of Raman spectra but

also laser-induced damages of quartz window of the Raman cell.

Generation of 1.56-μm heat pulse

The 1.56-μm pulse was generated by stimulated Raman scattering (SRS) in D_2 gas (ν = 2987 cm^{-1}) as the first Stokes-shifted line from the fundamental of a Q-switched Nd:YAG laser (GCR-150, Spectra Physics, Mountain View, CA) with 9-ns width (full width half maximum) at 10 Hz. To get it with high energy and high stability, the idea of the SRS seeding and amplification (Bisson, 1995) was incorporated. The optical alignment adopted in this experiment is illustrated in Fig. 2. The fundamental (1064 nm) of the Q-switched Nd:YAG laser was split into 1:5 by a beam-splitter (BS) with variable reflection ratio. The weak portion was focused by a lens (L1) into a Raman shifter (RS1), which is a 1.0-m-long gas cell (diameter = 12 mm) containing D_2 gas with 3.5 MPa. This yields a seed pulse at 1.56 μm through SRS (the first Stokes line). This seed pulse was collimated once with a convex lens (L2) and then expanded to the same size as the other portion of the split beam with a combination of a concave and convex lens (L3, L4). The seed pulse was overlain on the fundamental pulse spatially and temporarily by a dichroic mirror (DM) and focused by a lens (L5) into another Raman shifter (RS2), which is 1.1 m long (diameter = 20 mm) and contains D_2 gas with 3.5 MPa.

The 1.56-μm seed pulse thus generated was amplified by RS2. The split ratio of the fundamental was finely adjusted at this stage so that the final output energy of the 1.56-μm pulse could be maximized. This configuration of the seeding and amplification system enabled us to obtain the energy as large as 135 mJ for the 1.56-μm pulse from the pump pulse with 560 mJ at 1064 nm, 10 Hz (Conversion efficiency, 24%). The size of the heat pulse at the sample point was determined to be 1.4 mm in terms of a diameter on a burning paper. The temporal width of the 1.56-μm pulse was 9 ns and the energy fluctuations among individual pulses were less than 10%.

Determination of transient temperature

The transient temperature of the laser-illuminated volume of the sample following illumination of the heat pulse was determined with the intensity ratio of anti-Stokes to Stokes bands of Na_2MoO_4 in an aqueous solution, which were excited with another laser for variable delay times (Δt) after the illumination of the 1.56-μm pulse. The intensity (photon-counting rate) of anti-Stokes (I_{aS}) and Stokes (I_S) bands of a given molecular vibration with a wavenumber of ν_0 is related to the instantaneous temperature (T) by (Rassat and Davis, 1994),

$$\left(\frac{I_{aS}}{I_S}\right) = \left(\frac{\nu + \nu_0}{\nu - \nu_0}\right)^3 \exp\left(-\frac{hc\nu_0}{k_B T}\right), \quad (1)$$

where ν and k_B are a Raman excitation wavenumber and Boltzmann factor, respectively. The basic assumption for Eq. 1 is Boltzmann distribution among vibrational freedoms, and usually it is satisfied within a subnanosecond in the liquid phase. In the practical use of Eq. 1, it is more convenient to determine the amount of temperature rise (ΔT) than the absolute temperature. Supposed that the sample is initially placed in thermal equilibrium at T_0 and raised by ΔT upon illumination of the heat pulse, the measurements of Raman intensities at the initial stage, $(I_{aS}/I_S)_{T_0}$, and a transient state $(I_{aS}/I_S)_{T_0+\Delta T}$, give ΔT by

$$\ln\left(\frac{I_{aS}}{I_S}\right)_{T_0+\Delta T} - \ln\left(\frac{I_{aS}}{I_S}\right)_{T_0} = -\frac{hc\nu_0}{k_B}\left(\frac{1}{T_0 + \Delta T} - \frac{1}{T_0}\right). \quad (2)$$

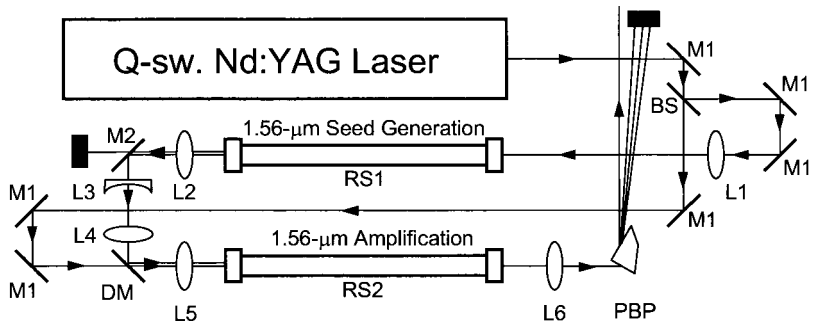

FIGURE 2 Schematic diagram of the 1.56-μm pulse-generation system with the stimulated Raman seeding and amplification technique. RS1, D_2 gas cell (3.5 MPa) with length of 1.0 m and diameter of 12 mm; windows, quartz with diameter of 25.9 mm and thickness of 20 mm. RS2, D_2 gas cell (3.5 MPa) with length of 1.1 m and diameter of 20 mm; windows, quartz with diameter of 38.1 mm and thickness of 19.1 mm; M1, mirror for 1064 nm; M2, mirror for 1.56 μm; BS, beam splitter with variable reflection ratio; DM, dichroic mirror with high reflectance at 1.56 μm and high transmittance at 1064 nm; L1, L2, L4, L5, L6, plano-convex lenses; L2, plano-concave lens; PBP, Pellin Broca prism.

Temperature jump cell

It is quite important to heat the sample uniformly, but, in practice, the intensity of a heat pulse decreases because of absorption as it proceeds from the surface to the inside of the sample. To overcome this problem, we adopted a counter-propagating geometry of two heat pulses. The 1.56-μm beam was split into two equal portions with a 50:50 beam splitter, and the 2-mm-thick sample cell with quartz windows was illuminated from both sides by the two beams. The sample solution was stirred with a teflon-coated magnet bar to avoid illumination of the same volume twice by successive heat pulses. The sample cell was held with brass blocks kept at T_0 by circulation of temperature-controlled water. A thermal-conductive sheet was inserted between the cell and the brass blocks to improve thermal exchange. The steady-state Raman spectra at given temperature was obtained by changing T_0. For the T-jump experiments, T_0 was kept at 25.0 and 59.0°C for the measurements of molybdate and RNase A solutions, respectively. Fluctuations of T_0 were less than 0.2°C in all the experiments.

Measurements of time-resolved Raman spectra

Raman scattering was excited by the second harmonic (532 nm) of another Q-switched Nd:YAG laser (GCR-11, Spectra Physics, Mountain View, CA) with the pulse width of 7 ns. The delay time of the Raman probe pulse from the 1.56-μm heat pulse was controlled by a pulse generator (DG535, Stanford Research Systems, Sunnyvale, CA). The scattered light at right angle was collected and dispersed with a 25-cm single imaging spectrograph (250IS, Chromex, Albuquerque, NM). Between its entrance slit and the sample, another rectangular slit, a holographic notch filter (Super Notch-Plus, Kaiser Optical Systems, Ann Arbor, MI) and an iris were placed to reduce the stray light. The dispersed light was detected with an intensified photodiode array (model 1421, EG&G PARC, Princeton, NJ).

One cycle of the T-jump experiment involves the series of spectral measurements along increasing Δt and decreasing Δt, and, in addition, the probe-only spectrum was measured at the end of the individual series. The Raman spectra presented are an average over 9 and 20 cycles for molybdate ions and RNase A, respectively.

RESULTS

Figure 3 shows the stationary anti-Stokes and Stokes Raman spectra of Na_2MoO_4 1.5 M aqueous solution at 77.4 (*a*) and 20.1°C (*b*), respectively. Two Raman bands are seen at 317 and 897 cm^{-1}, and the spectral intensities are normalized by the Stokes 897 cm^{-1} band at 20.1°C. The time-resolved Raman spectra were observed for various Δt values following illumination of the heat pulse, and transient temperature difference ΔT were obtained from I_{aS} and I_S, according to

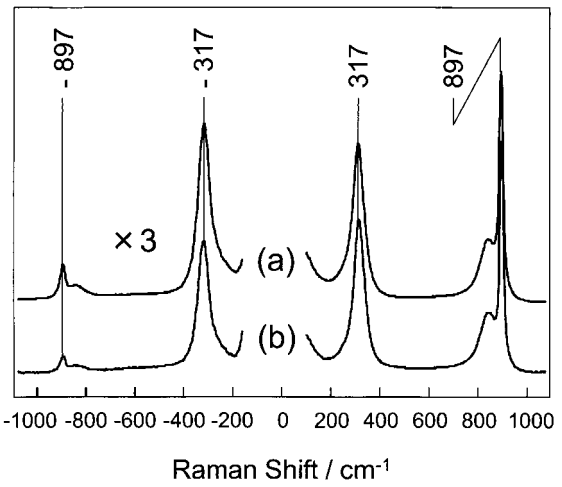

FIGURE 3 Stationary-state Stokes and anti-Stokes Raman spectra of Na_2MoO_4 1.5 M aqueous solution excited at 532 nm. (*a*) 77.4 ± 0.2°C, (*b*) 20.1 ± 0.1°C. Experimental conditions: exposure time, 20 s; repetition, 60. The spectral contribution from water and cell had been subtracted. The intensity of spectra is normalized to the Stokes 897 cm^{-1} band. The anti-Stokes Raman spectra are vertically magnified by three times of the Stokes spectra.

Eq. 2. The average values of ΔT derived from the two bands are plotted against Δt in Fig. 4. The differences in estimation of ΔT from the two bands are reflected by error bars. Temperature rise as large as 9°C was achieved in the present apparatus.

When the cylindrical volume, whose diameter and length are 1.4 mm (size of the heat pulse) and 2 mm (sample thickness), respectively, absorbs 84% of the total heat pulse (135 mJ), the temperature rise expected for the solution with specific heat of 1 cal/°C is 8.8°C, which is in good agreement with the experimental value. The broken line in Fig. 4 *A* displays the cross-correlation function of the heat pulse and Raman probe pulse. The temporal behavior of the temperature rise calculated from the cross-correlation function is represented by the solid line in Fig. 4 *A*, in which the temperatures before and after the T-jump were fixed to the experimental values, and the inclination was calculated. The calculated temporal behavior almost completely reproduces the observed one. This means that the energy of the heat pulse was converted to thermal energy within its pulse width and that the nanosecond T-jump was achieved as designed. It is noted, however, that the temperature in the negative delay time region is higher than T_0 by 3°C. This was due to insufficient heat conductance between the solution and the cell holder under 10 Hz of repetition rate, and, as a result, the solution is slightly heated during the pump-probe measurements. However, the probe-only spectrum at the end of the series indicated the recovery of temperature to T_0. Because the experiments for RNase A were performed under the exactly identical conditions except for T_0, Fig. 4 *A* serves as a calibration curve of temperature in this experiment.

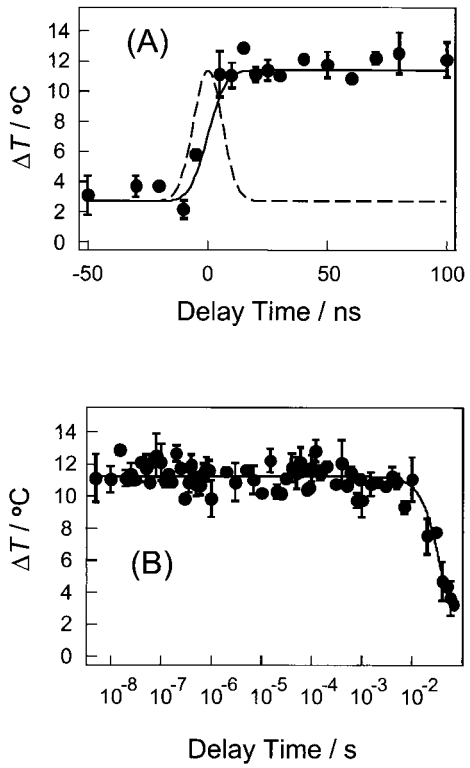

FIGURE 4 (*A*) Observed temperature rise and (*B*) its long time behavior of the Na_2MoO_4 solution after one shot of heat pulse. Filled circles denote the observed temperature rise determined with the anti-Stokes/Stokes intensity ratios of two bands of molybdate ions in water. The error bars reflect the differences in estimation of ΔT from the two bands. (*A*) Broken line and solid line show the cross correlation function of the heat and probe pulses and the expected temperature rise calculated from the correlation function without any fitted parameter, respectively. (*B*) Solid line shows the expected temperature recovery calculated from the rate of volume exchange by stirring.

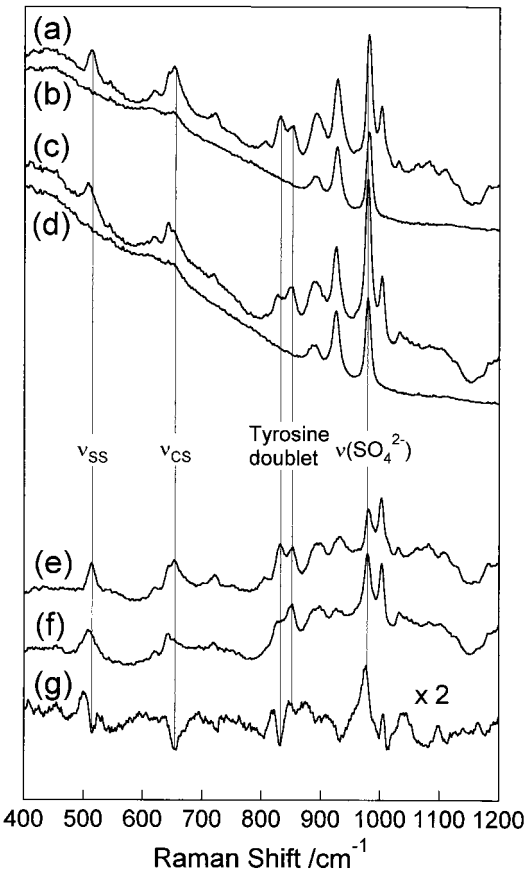

FIGURE 5 Steady Raman spectra of RNase A and buffer solution (200 mM acetate buffer, pH 5.0 containing 50 mM Na_2SO_4); Spectra (*a*, *b*, and *e*) were obtained at 20.0°C, and spectra (*c*, *d*, and *f*) at 71.0°C. Trace (*g*) shows the temperature-difference spectrum of RNase A, $(g) = 2 \times [f–e]$. Spectra (*a*) and (*c*) are the raw Raman spectra of RNase A containing the buffer solution, and spectra (*b*) and (*d*) are those of the buffer solution only. Spectra (*e*) and (*f*) were obtained by subtraction of buffer-solution spectra [(*b*) and (*d*)] from the raw RNase A spectra [(*a*) and (*c*)] at each temperature; $(e) = (a)–(b)$ and $(f) = (c)–(d)$. Hence the difference spectrum (*g*) of RNase A does not include the spectral changes of buffer solution. Experimental conditions: exposure time, 30 s; repetition, 60; laser, 532 nm, 5 mJ/pulse.

Figure 4 *B* shows the recovery of temperature observed for longer delay times. The elevated temperature remained unchanged up to 10 ms. The solid line in Fig. 4 *B* indicates the curve of ΔT that is calculated for the replacement of the heated volume with fresh solution through stirring. The good agreement of the solid line with the experimental points means that thermal diffusion can be neglected in 100 ms. Because the pulse-to-pulse interval is 100 ms, the temperature recovery around 10 ms corroborates the present set up of experimental conditions.

Figure 5 displays the steady-state Raman spectra of RNase A and buffer solution observed at 20.0°C (*a*, *b*, and *e*) and 71.0°C (*c*, *d*, and *f*) and the difference spectrum of RNase A [$g = 2 \times (f–e)$]. Spectra *a* and *c* are the raw Raman spectra of RNase A containing the contribution from the buffer solution (200 mM acetate buffer with 40 mM Na_2SO_4) and spectra *b* and *d* show those of the buffer solution only. Spectra *e* and *f* were obtained by subtraction of buffer-only spectra [*b* and *d*] from the raw RNase A spectra [*a* and *c*] at each temperature. Hence, the difference spectrum, *g*, of RNase A does not include the spectral changes of buffer solution. The vibrational assignments of well-established Raman bands (Harada and Takeuchi, 1986) are designated in Fig. 5. Upon the temperature change from 20.0 to 71.0°C, the ν_{SS} band around 510 cm^{-1} exhibits a frequency shift toward lower frequencies and broadening (from 14 to 26 cm^{-1} in terms of half-height width), while the ν_{CS} band around 655 cm^{-1} shows intensity reduction. The SO_4^{2-} band around 980 cm^{-1} shows intensity increase. The intensity ratio of the tyrosine doublet at 831/851 cm^{-1} changes from 1.4 to 0.8, indicating the change of hydrogen bonding of tyrosine residues (Siamwiza et al., 1975). These changes qualitatively agree with the reported results (Chen and Lord, 1976).

Figure 6 shows the transient Raman spectra of RNase A upon T-jump from 62 to 71°C. Spectra *a–d* were observed for Δt of −100 ns, 200 ns, 100 μs, and 5 ms, respectively, whereas spectrum *e* represents the probe-only spectrum observed in the cycle of T-jump experiments. For comparison, the steady-state spectra at 59.0 and 71.0°C are also included as spectra *f* and *g*, respectively. In all of them, the buffer-only spectrum, measured under the same condition, had been subtracted. Apparently, all the spectra except for spectrum *g* appear similar, but their changes can be revealed by difference calculations.

Figure 7 displays the difference spectra that were calculated from raw spectra, and, therefore, the contributions from buffer solution had not been subtracted. The time-resolved spectra are represented as the difference from the probe-only spectrum measured at T_0 (59°C). Accordingly, spectra *a–d* correspond to $\Delta t = -100$ ns, 200 ns, 100 μs, and 5 ms, respectively. Spectra *e* and *f* delineate the steady-state temperature-difference spectra of 62.0–59.0°C and 71.0–59.0°C, respectively. The stationary-state temperature difference between the buffer-only spectra at 71.0 and 59.0°C is also represented by spectrum *g* for reference. This is the maximum contribution from the temperature dependence of the buffer spectrum. Spectral changes of buffer solution are small except for the bands of acetate (~925 cm^{-1}) and sulfate (~980 cm^{-1}), which exhibited appreciable temperature dependence.

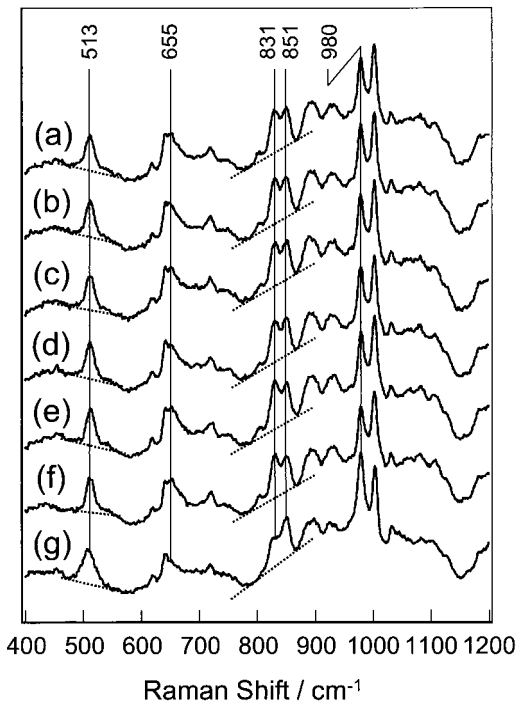

FIGURE 6 Time-resolved Raman spectra of RNase A upon T-jump. (*a*) $\Delta t = -100$ ns, (*b*) $\Delta t = 200$ ns, (*c*) $\Delta t = 100$ μs, (*d*) $\Delta t = 5$ ms, (*e*) probe only at T_0 (59.0°C), (*f*) stationary state spectrum at 59.0°C, (*g*) stationary state spectrum at 71.0°C. Buffer spectra, which were obtained under the same experimental conditions as respective raw spectra of RNase A solution, had been subtracted in all the spectra (*a*)–(*g*). Broken lines designate the base lines assumed for the calculations of intensity and bandwidth.

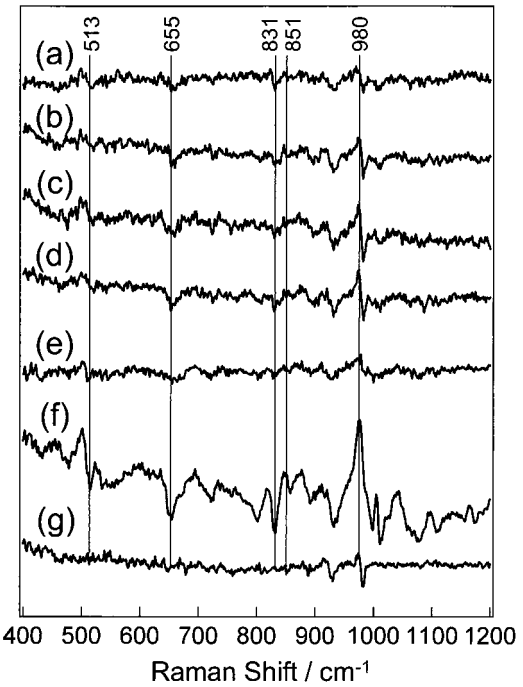

FIGURE 7 Difference spectra of RNase A upon T-jump; (*a*)–(*d*) pump/probe–probe-only; (*e*)–(*g*) steady-state temperature-difference spectra. (*a*) $\Delta t = -100$ ns, (*b*) $\Delta t = 200$ ns, (*c*) $\Delta t = 100$ μs, (*d*) $\Delta t = 5$ ms, (*e*) 62.0–59.0°C, (*f*) 71.0—59.0°C, (*g*) buffer-only 71.0–59.0°C. Because raw spectra were used for these calculations, spectra (*a*)–(*f*) contain spectral changes of buffer solution.

Spectrum *a* at −100 ns is almost the same as spectrum *e*. This is compatible with the fact that the reference temperature in the repeated T-jump experiment is 3°C higher than T_0. Spectrum *b* exhibits differential peaks at 925 cm^{-1} and 980 cm^{-1}, which are attributed to acetate ions and sulfate ions, respectively. These amounts of spectral differences are close to the sum of spectral changes of buffer solution (71.0–62.0°C) and that of RNase A raw spectrum for $\Delta t = -100$ ns (*a*), indicating that the temperature is definitely raised at $\Delta t = 200$ ns (*b*). In addition to the buffer peaks, spectrum *b* contains the contribution from the C–S stretching around 655 cm^{-1}. Spectrum *c* is slightly noisier than spectra *b* and *d* because of the appearance of the effects of the shock wave generated by the heat pulse, which practically increases Rayleigh scattering. Despite the efforts to remove it through optical alignments and filtering, it remained. Therefore, this contribution has been removed by subtraction of water spectrum measured under similar conditions. Anyway, this does not affect the difference intensity of any particular peak except for increased noises. Spectrum *c* exhibits an increase of differential patterns for the SO_4^{2-} band and the intensity reduction for the ν_{CS} band. Spectrum

d is nearly the same as spectrum *c* but is distinct from spectrum *f*, suggesting that the conformational change does not proceed largely between 100 μs and 5 ms.

For detailed analysis of the transient spectra of RNase A, a part of the difference spectra is delineated in an expanded scale in Fig. 8, where *panels A* and *B* denote the C–S and SO_4^{2-} stretching regions, respectively. For comparison, transient and stationary difference spectra of the buffer solution only are shown in *panel C*, where the ordinate and abscissa scales are the same as those of *panel B*. The delay times or stationary-state temperature in *panel C* are the same as those designated in *panel B*. In the spectra shown in *panel B*, the contributions from the temperature dependence of buffer-only spectrum (*panel C*) had been subtracted. The base lines used for quantitative evaluation of changes are shown by broken lines. The temporal changes in difference spectra are clearer in Fig. 8 than in Fig. 7. The intensity increase of the SO_4^{2-} band in *panel B* is seen in the spectrum

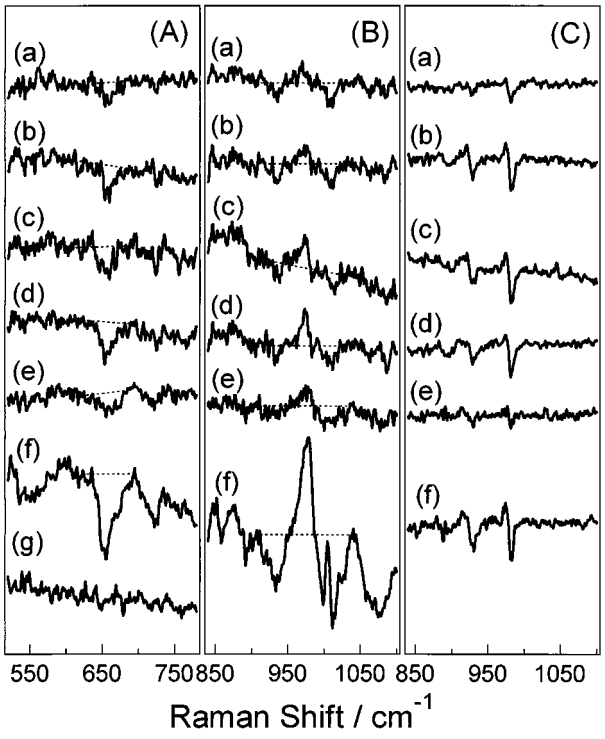

FIGURE 8 The expanded difference Raman spectra of RNase A upon T-jump for the (*A*) C–S stretching and (*B*) SO_4^{2-} stretching regions and (*C*) those of buffer solution only upon T-jump; Spectra *a–d* show the differences, pump/probe–probe-only, and spectra *e–g* show the stationary-state temperature-difference spectra; (*a*) $\Delta t = -100$ ns, (*b*) $\Delta t = 200$ ns, (*c*) $\Delta t = 100$ μs, (*d*) $\Delta t = 5$ ms, (*e*) 62.0–59.0°C, (*f*) 71.0–59.0°C, and (*g*) buffer-only 71.0–59.0°C. Buffer difference spectra *a–f* in panel (*C*) were observed under the same conditions as those for (*B*). In practice, spectra in panel (*B*) were obtained by subtracting spectra *a–f* in panel (*C*) from spectra *a–f* in Fig. 7, respectively, although such subtraction had not been done for spectra in panel (*A*). The ordinate and abscissa scales in panels (*B*) and (*C*) are the same. The broken lines denote the base lines used for the difference intensity calculations.

for $\Delta t = 100$ μs (*c*) and grows until $\Delta t = 5$ ms (*d*), whereas that in *panel C* occurs in the spectrum for $\Delta t = 200$ ns (*b*) and remains unchanged until 5 ms (*d*). Therefore, the transient intensity increase in *panel B* is distinct from that of buffer solution.

The temporal spectral changes were calculated as area intensities of the difference peaks, and the results are illustrated in Fig. 9, where the intensity reduction of the ν_{CS} band in the stationary state spectra is also plotted against temperature in *panel A*. The intensity changes in the transient spectra are the quantities relative to the change between the stationary-state spectra at 59.0 and 71.0°C, which were obtained from Fig. 8 *A*, although the positions along the abscissa are arbitrary. Here, the probe-only spectrum at T_0 (59.0°C) was used as the reference. The spectrum of $\Delta t = -100$ ns exhibits 20% reduction of intensity, and it corresponds to that of the stationary-state spectrum at 62.0°C, in good agreement with the calibration using MoO_4^{2-} ions. For $\Delta t = 200$ ns, the intensity decreased further by 10%, but the amount of intensity decrease was 40% of the stationary-state difference even at 5 ms. In contrast, the intensity increase of the SO_4^{2-} bands for $\Delta t = -100$ ns is small, and it is consistent with the difference in the stationary-state spectrum between 59.0 and 62.0°C as shown in spectrum *e* of Fig. 8 *B*. Its intensity increase starts from $\Delta t = 100$ μs as illustrated in Fig. 9 *B*, where the intensity changes normalized to the positive part of spectrum *f* in Fig. 8 *B* are designated.

DISCUSSION

Temperature jump in RNase A solution

Temperature rise by laser-induced T-jump can be determined from the energy of the heat pulse and the heated volume of the sample as demonstrated for the MoO_4^{2-} solution (Fig. 4 *A*). Nevertheless, it is a critical problem whether the laser-induced T-jump with the 1.56-μm pulse brings about as high and as rapid temperature rise in the protein solution as in the MoO_4^{2-} solution. In nonresonant Raman scattering measurements, however, spectra of both RNase A and temperature reference material cannot be obtained simultaneously, because the former is much weaker in Raman intensity than the latter. Hence, the transient temperature behavior was examined for the mixed solution of 7 mM RNase A with 0.42 M Na_2MoO_4 (pH 5.0) at 59.0°C by laser-induced T-jump, where the beam size of the heat pulse was the same as that used in the T-jump experiments of the MoO_4^{2-} and the RNase A solutions. From the 317 and 897 cm^{-1} bands of MoO_4^{2-} in the transient spectra of this solution, which almost consisted of MoO_4^{2-} bands (not shown), the temperature rise was determined. The observed temperatures are plotted against the delay time in Fig. 10, where the abscissa scale is linear in a short time region (*A*) but logarithmic in a longer time region

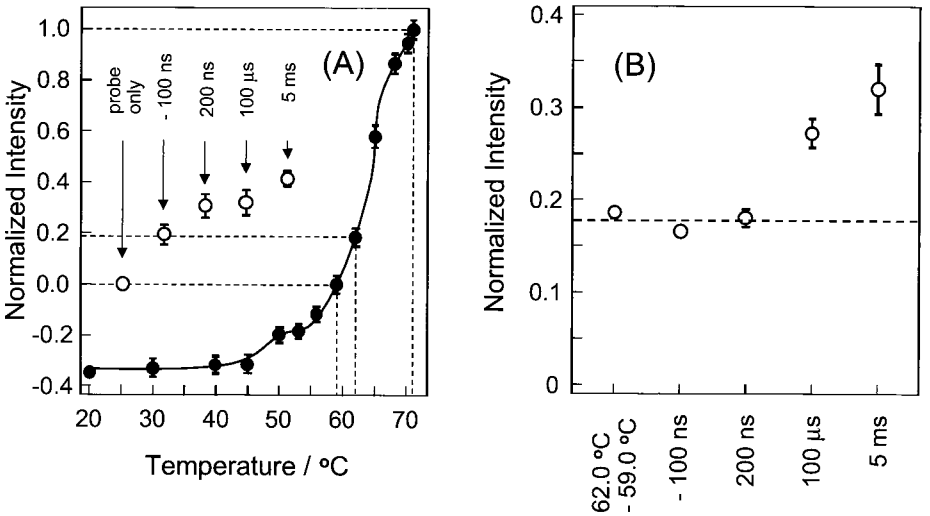

FIGURE 9 (*A*) Intensity decrease of the ν_{CS} bands and (*B*) intensity increase of SO_4^{2-} bands of RNase A upon T-jump (*open circles*) and upon steady-state temperature change (*closed circles*).

(*B*). It was thus confirmed that the temperature rise of 9 ± 1°C, at least, was accomplished within 20 ns, and that temperature in the negative-delay region was 2.5 ± 1°C higher than the reference temperature (59.0°C). This result agrees with the transient temperature behavior of the MoO_4^{2-} solution (1.5 M) without protein, shown in Fig. 4 *A*.

However, we cannot rule out a possibility that the protein stability increases due to MoO_4^{2-} ions added, and, as a result, the melting did not occur in this temperature range. This would mean that, in the absence of the heat energies absorbed by thermal unfolding, the temperature rises are identical between the MoO_4^{2-} solutions with and without the protein. From the enthalpy changes of 757 kJ mole^{-1} involved in the thermal unfolding of RNase A at pH 5.0 (Tsong et al., 1970; Privalov, 1990), the absorbed heat resulting from the thermal unfolding of 7 mM RNase A solution in the laser-heated volume can be estimated to be 16 mJ for the present T-jump experiments (Figs. 6, 7, and 8). The estimated energy is 12% of the heat-pulse energy (135 mJ) and would be totally absorbed when thermal unfolding of RNase A is completed. Even in this case, 88% of the heat pulse energy can be used to raise temperature similar to the case of a simple MoO_4^{2-} solution. In fact, the conformational changes of RNase A observed were small within the initial 5 ms after the T-jump, and, hence, the actual heat energy absorbed would be much less than that thus estimated. Therefore, the temperature rise in the RNase A solution by laser induced T-jump is considered to be close to that observed for the MoO_4^{2-} solution ($\Delta T = 9$°C).

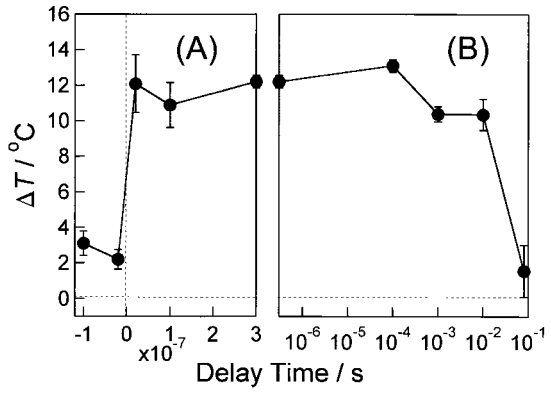

FIGURE 10 Temperature rise observed for the mixture solution of MoO_4^{2-} ions (0.42 M) with RNase (7 mM) under the same experimental conditions as those for Fig. 4 *A*. The scale of abscissa is (*A*) linear in a shorter time region but (*B*) logarithmic in a longer time region.

Disulfide conformations

Sugeta et al. (1972, 1973) and Sugeta (1975) studied the relationship between the S–S stretching frequency and conformation, and interpreted it in terms of dihedral angles around the three successive bonds of C–C-S-S-C-C; 508–512 cm^{-1} for GGG, 523–528 cm^{-1} for TGG, and 540–545 cm^{-1} for TGT (T, *trans*; G, *gauche*). They also determined with diethyldisulfide that the GGG conformation is more stable by 2.5 kJ/mol than TGG. The TGT form has not been identified. The ν_{SS} modes of RNase A have been observed at 514 cm^{-1} at room temperature and no peaks at 520–545 cm^{-1}, indicating that the four disulfide bonds adopt the GGG conformation. This conformational assignment of disulfide bridges agrees with the x-ray crystallographic structure illustrated in Fig. 1, where all the four disulfide bridges form the GGG conformation.

The ν_{SS} bands in Fig. 6 were fitted by a single Gaussian function under the assumption of inclined straight base line. Their peak frequencies and bandwidths were determined for both transient and steady-state spectra and are plotted against temperature in Fig. 11. The peak frequency differs between the probe-only spectrum and that for $\Delta t = -100$ ns, but they are in reasonable agreement with the steady-

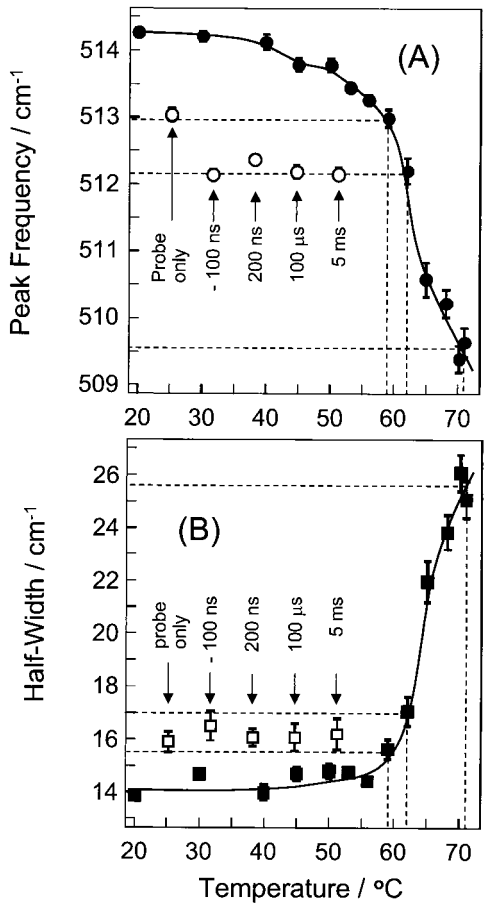

FIGURE 11 Peak-shift and band-broadening of the ν_{SS} bands of RNase A upon T-jump (*open symbols*) and upon steady-state temperature change (*closed symbols*). (*A*) Peak frequency and (*B*) half-width.

state spectra measured at 59.0 and 62.0°C, respectively. The ν_{SS} frequency in the transient state spectra did not change in 5 ms. The half-width becomes larger at higher temperatures in the steady-state spectra, and its behavior is close to that of peak frequencies. However, in the transient spectra, the half-width also remained unchanged until 5 ms. These results mean that a conformational change around the four disulfide bridges of cysteine residues does not take place in the initial 5 ms of thermal unfolding. This conclusion is compatible with the notes (Talluri et al., 1994; Laity et al., 1997) that disulfide bridges play a critical role in the stabilization of RNase A.

Upon the temperature rise from 59 to 71°C, the ν_{SS} frequency decreased from 513 to 509 cm^{-1}. This implies that the conformation changes within the category of the GGG conformation. It is plausible that the disulfide moiety in native RNase A has some strain at room temperature, but that the strain disappears upon relaxation of the tertiary structure at higher temperatures, and the C_α–$C_\beta H_2$-S_γ-S'_γ-$C'_\beta H_2$-C'_α moiety approaches more to the true GGG conformation. However, band broadening indicates the presence of various conformations at higher temperatures.

Cysteine residues also give rise to the C–S stretching bands around 630–750 cm^{-1}. The correlation between the C–S stretching frequency and the conformation of X-C-CH_2-S- has been studied with dialkyl-disulfide molecules as model compounds of the disulfide bridge (Sugeta et al., 1972, 1973; Sugeta, 1975). The ν_{CS} frequency is sensitive to an atom (X) at the *trans* position of S atom; 630–670 cm^{-1} for X = H (P_H) and 700–745 cm^{-1} for X = C (P_C), where P_X denotes that the atom X is present at the *trans* position of the S atom. From the x-ray crystallographic structure of RNase A (Howlin et al., 1989), all the eight cysteine residues adopt the P_C conformation regarding the X-C_α–$C_\beta H_2$-S- group. Therefore, it is considered that the C–S stretch of cysteine residues hardly contributes to the intensity reduction at 655 cm^{-1} in the transient and stationary spectra of RNase A in Fig. 9 *A*.

Conformation of methionine

The fact that the ν_{CS} modes of cysteine residues do not give rise to the 655-cm^{-1} band leads us to presume that the intensity reduction of ν_{CS} bands around 655 cm^{-1} is due to the C–S stretching of methionine residues. Actually, RNase A has four methionine residues; (Met-13, -29, -30, and -79). It has been demonstrated from studies of model monosulfide compounds having the X-C-CH_2-S-CH_3 structure that the ν_{CS} frequency of CH_2-S group is sensitive to an atom (X) at the *trans* position of the S atom; 640–680 cm^{-1} for X = H (P_H), and 740–760 cm^{-1} for X = C (P_C) (Nogami et al., 1975a,b,c). Methyl-propylsulfide, which is the closest model compound in their studies to the side chain of a methionine residue, gives rise to Raman bands at 645 and 667 cm^{-1} for the P_H-G and P_H-T conformations, respectively. In contrast, the ν_{CS} frequency of the S-CH_3 group is fairly independent of its conformation (700–725 cm^{-1}). Consequently, it is presumed that the side chain conformation of some methionine residues changes in the initial stage of unfolding. From the x-ray crystallographic structure (Howlin et al. 1989), the side chains (X-$C_\beta H_2$-$C_\gamma H_2$-S_δ-$C_\epsilon H_3$) of Met-13, -29, and -30 adopt the P_H-G conformation, and that of Met-79 adopts the P_C-T conformation. Hence, Met-13, -29, and -30 are considered as the candidates that underwent some conformational changes of side chains in the initial stage of unfolding. Because the -$C_\gamma H_2$-S_δ-$C_\epsilon H_3$ side chain has no particular interactions with other residues, it is reasonable that some changes of packing of this group in the tertiary structure relaxation starts at 200 ns following T-jump.

Conformational change of tyrosine side chain

RNase A has six tyrosine residues (Tyr-25, -73, -76, -92, -97, and -115). The tyrosine doublet at 831 and 851 cm^{-1} arises from the Fermi resonance between the ring-breathing

fundamental and an overtone of out-of-plane ring deformation vibration (Siamwiza et al., 1975). The relative intensity of two bands sensitively depends on the proximity of the two unperturbed frequencies and thus on the hydrogen bonding conditions of the phenol side-chain. In fact, the tyrosine doublet shows clear spectral changes between 20.0 and 71.0°C as demonstrated in Fig. 5. For quantitative evaluation of the spectral changes, the spectra in the 780 to 870 cm^{-1} region in Fig. 6 were fitted with triple Gaussian functions with inclined straight base line as drawn in the spectra (Fig. 6). Two Gaussians reflect the tyrosine doublet and the other corresponds to a weak peak around 800 cm^{-1}. The intensity ratios of the low- to high-frequency components are plotted against temperature in Fig. 12. The intensity ratios of steady-state spectra exhibit a large change with a midpoint at 62°C similar to the changes of the ν_{CS} (Fig. 9 *A*) and ν_{SS} Raman bands (Fig. 11). In the time-resolved spectra, the ratios in the spectrum for $\Delta t = -100$ ns and in the probe-only spectrum are different in consequence of the 3°C difference between 59.0 and 62.0°C. However, the intensity ratios little change until 5 ms as illustrated in Fig. 12, indicating that the conformational changes of the side chain of tyrosine residues do not take place within the initial 5 ms of unfolding. The present results give some information on structural changes occuring in the time region before that of the kinetic UV absorption study (Hagerman and Baldwin, 1976).

Sulfate ions

RNase A is considered to bind three phosphodiester groups of RNA when it catalyzes the hydrolysis reaction of RNA (Arus et al., 1982). In the absence of phosphate ions, as so in this experiment, three sulfate anions are thought to occupy the three phosphate sites. Transient intensity increase around 980 cm^{-1} demonstrated in Fig. 9 *B* was caused by the sulfate ions occupying the active site but not by free sulfate ions initially present in the buffer solution. This is evident from the comparison of the spectra shown in *panels B* and *C* in Fig. 8. One may argue a possibility that it reflects the free sulfate ions that have been released from RNase A due to the base temperature difference (3°C). However, this possibility is unlikely on account of the following reasons: 1) the transient change of the band due to the released sulfate ions, if present, should appear in the spectrum for $\Delta t = 200$ ns similar to that for the buffer spectrum *b* of Fig. 8 *C*; and 2) the transient change of the band around 980 cm^{-1} in Fig. 8 *B* is not recognized in spectrum *b* for $\Delta t = 200$ ns but appreciably in spectra *c* for $\Delta t = 100$ μs and *d* for $\Delta t = 5$ ms. Furthermore, careful examination of the band position in the transient spectra seemed to exhibit a small but definite low-frequency shift ($\sim$5 cm^{-1}) with time. Therefore, it is concluded that the transient intensity increase around 980 cm^{-1} originates from the sulfate ions occupying the active site of RNase A and reflects the temporal changes of the structure around the site. This may mean that the protein conformation near the active site is more flexible than the other parts, and, accordingly, its structural response to raised temperature is faster.

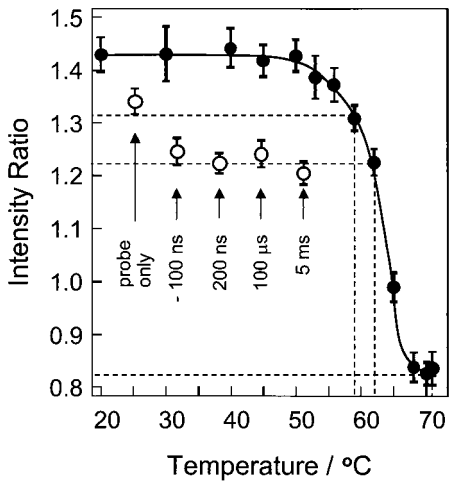

FIGURE 12 Intensity ratio of tyrosine doublet (I_{831}/I_{851}) of RNase A upon T-jump (*open circles*) and upon steady-state temperature change (*closed circles*).

The authors are indebted to Prof. Shingo Tsuyama of Osaka Prefecture University (Dept. of Veterinary Science) for his help in purification of RNase A and to Prof. Atsuo Tamura of Kobe University (Faculty of Science) for his advice on sample treatments.

This study was supported by grant-in-Aid for Scientific Research from the Ministry of Education, Science, Sports, and Culture, Japan to T.K. (10480187).

REFERENCES

Anfinsen, C. B. 1973. Principles that govern the folding of protein chains. *Science.* 181:223–230.

Anfinsen, C. B., and H. A. Scheraga. 1975. Experimental and theoretical aspects of protein folding. *Adv. Protein Chem.* 29:205–300.

Arus, C., L. Paolillo, R. Llorens, R. Napolitano, and C. M. Cuchillo. 1982. Evidence on the existence of a purine ligand induced conformational change in the active site of bovine pancreatic ribonuclease A studied by proton nuclear magnetic resonance spectroscopy. *Biochemistry.* 21: 4290–4297.

Ballew, R. M., J. Sabelko, and M. Gruebele. 1996. Direct observation of fast protein folding: the initial collapse of apomyoglobin. *Proc. Natl. Acad. Sci. USA.* 93:5759–5764.

Barksdale, A. D., and J. E. Stuehr. 1972. Kinetics of the helix-coil transition in aqueous poly(L-glutamic acid). *J. Am. Chem. Soc.* 94:3334–3338.

Bisson, S. E. 1995. Parametric study of an excimer-pumped, nitrogen Raman shifter for lidar applications. *Appl. Opt.* 34:3406–3412.

Burke, J. J., G. G. Hammes, and T. B. Lewis. 1965. Ultrasonic attenuation measurements in poly-L-glutamic acid solutions. *J. Chem. Phys.* 42: 3520–3525.

Chen, M. C., and R. C. Lord. 1976. Laser Raman spectroscopic studies of the thermal unfolding of ribonuclease A. *Biochemistry.* 15:1889–1897.

Cummings, A. L., and E. M. Eyring. 1975. Helix-coil transition kinetics in aqueous poly(α, L-glutamic acid). *Biopolymers.* 14:2107–2114.

Eaton, W. A., V. Munoz, P. A. Thompson, E. R. Henry, and J. Hofrichter. 1998. Kinetics and dynamics of loops, α-helices, β-hairpins, and fast-folding proteins. *Acc. Chem. Res.* 31:745–753.

Gilmanshin, R., S. Williams, R. H. Callender, W. H. Woodruff, and R. B. Dyer. 1997. Fast events in protein folding: relaxation dynamics of secondary and tertiary structure in native apomyoglobin. *Proc. Natl. Acad. Sci. USA.* 94:3709–3713.

Gruebele, M., J. Sabelko, R. Ballew, and J. Ervin. 1998. Laser temperature jump induced protein refolding. *Acc. Chem. Res.* 31:699–707.

Gruenewald, B., C. U. Nicola, A. Lustig, G. Schwarz, and H. Klump. 1979. Kinetics of the helix-coil transition of a polypeptide with non-ionic side groups, derived from ultrasonic relaxation measurements. *Biophys. Chem.* 9:137–147.

Hagerman, P. J., and R. L. Baldwin. 1976. A quantitative treatment of the kinetics of the folding transition of ribonuclease A. *Biochemistry.* 15: 1462–1473.

Hammes, G. G., and P. B. Roberts. 1969. Dynamics of the helix-coil transition in poly-L-ornithine. *J. Am. Chem. Soc.* 91:1812–1816.

Harada, I., and H. Takeuchi. 1986. Raman and ultraviolet resonance Raman spectra of proteins and related compounds. *In* Advances in Spectroscopy. R. J. H. Clark and R. E. Hester, editors. John Wiley and Sons, New York. 13:113–175.

Hoffman, H., E. Yeager, and J. Stuehr. 1968. Laser temperature-jump apparatus for relaxation studies in electrolytic solutions. *Rev. Sci. Instrum.* 39:649–653.

Howlin, B., D. S. Moss, and G. W. Harris. 1989. Segmented anisotropic refinement of bovine ribonuclease A by the application of the rigid-body TLS model. *Acta Crystallog. Sect. A.* 45:851–861.

Konishi, Y., T. Ooi, and H. A. Scheraga. 1982. Regeneration of RNase A from the reduced protein: models of regeneration pathways. *Proc. Natl. Acad. Sci. USA.* 79:5734–5738.

Laity, J. H., C. C. Lester, S. Shimotakahara, D. E. Zimmerman, G. T. Montelione, and H. A. Scheraga. 1997. Structural characterization of an analog of the major rate-determining disulfide folding intermediate of bovine pancreatic ribonuclease A. *Biochemistry.* 36:12683–12699.

Lednev, I. K., A. S. Karnoup, M. C. Sparrow, and S. A. Asher. 1999. Nanosecond UV resonance Raman examination of initial steps in α-helix secondary structure evolution. *J. Am. Chem. Soc.* 121:4076–4077.

Li, Y. J., D. M. Rothwarf, and H. A. Scheraga. 1995. Mechanism of reductive protein unfolding. *Nature Struct. Biol.* 2:489–494.

Munoz, V., P. A. Thompson, J. Hofrichter, and W. A. Eaton. 1997. Folding dynamics and mechanism of β-hairpin formation. *Nature.* 390:196–199.

Nogami, N., H. Sugeta, and T. Miyazawa. 1975a. C–S stretching vibrations and molecular conformations of methyl propyl sulfide and related alkyl sulfides. *Chem. Lett.* 147–150.

Nogami, N., H. Sugeta, and T. Miyazawa. 1975b. C–S stretching vibrations and molecular conformations of isobutyl methyl sulfide and related alkyl sulfides. *Bull. Chem. Soc. Jpn.* 48:2417–2420.

Nogami, N., H. Sugeta, and T. Miyazawa. 1975c. Vibrational spectra and molecular structure of ethyl methyl sulfide. *Bull. Chem. Soc. Jpn.* 48:3573–3575.

Parker, R. C., L. J. Slutsky, and K. R. Applegate. 1968. Ultrasonic absorption and the kinetics of conformational change in poly-L-lysine. *J. Phys. Chem.* 72:3177–3186.

Phillips, C. M., Y. Mizutani, and R. M. Hochstrasser. 1995. Ultrafast thermally induced unfolding of RNase A. *Proc. Natl. Acad. Sci. USA.* 92:7292–7296.

Privalov, P. L. 1990. Cold denaturation of proteins. *Crit. Rev. Biochem. Mol. Biol.* 25:281–305.

Rassat, S. D., and E. J. Davis. 1994. Temperature measurement of single leviated microparticles using Stokes/anti-Stokes Raman intensity ratios. *Appl. Spectrosc.* 48:1498–1505.

Rothwarf, D. M., and H. A. Scheraga. 1991. Regeneration and reduction of native bovine pancreatic ribonuclease A with oxidized and reduced dithiothreitol. *J. Am. Chem. Soc.* 113:6293–6294.

Rothwarf, D. M., and H. A. Scheraga. 1993a. Regeneration of bovine pancreatic ribonuclease A. 1. Steady-state distribution. *Biochemistry.* 32:2671–2679.

Rothwarf, D. M., and H. A. Scheraga. 1993b. Regeneration of bovine pancreatic ribonuclease A. 4. Temperature dependence of the regeneration rate. *Biochemistry.* 32:2698–2703.

Sano, T., T. Yasunaga, Y. Tsuji, and H. Ushio. 1975. An optical rotation temperature jump apparatus for helix-coil transition of biopolymers. *Chem. Instrum.* 6:285–296.

Schwarz, G. 1965. On the kinetics of helix-coil transition of polypeptides in solution. *J. Mol. Biol.* 11:64–77.

Schwarz, G., and J. Seelig. 1968. Kinetic properties and the electric field effect of the helix-coil transition of poly(gamma-benzyl L-glutamate) determined from dielectric relaxation measurements. *Biopolymers.* 6:1263–1277.

Sela, M., and C. B. Anfinsen. 1957. Some spectrophotometric and polarimetric experiments with ribonuclease. *Biochim. Biophys. Acta.* 24: 229–235.

Siamwiza, M. N., R. C. Lord, M. C. Chen, T. Takamatsu, I. Harada, H. Matsuura, and T. Shimanouchi. 1975. Interpretation of the doublet at 850 and 830 cm^{-1} in the Raman spectra of tyrosyl residues in proteins and certain model compounds. *Biochemistry.* 14:4870–4876.

Staerk, H., and G. Czerlinski. 1965. Nanosecond heating of aqueous systems by giant laser pulses. *Nature.* 205:63–64.

Sugeta, H., A. Go, and T. Miyazaya. 1972. S–S and C–S stretching vibrations and molecular conformations of dialkyl disulfides and cystine. *Chem. Lett.* 83–86.

Sugeta, H., A. Go, and T. Miyazaya. 1973. Vibrational spectra and molecular conformations of dialkyl disulfides. *Bull. Chem. Soc. Jpn.* 46: 3407–3411.

Sugeta, H. 1975. Normal vibrations and molecular conformations of dialkyl disulfides. *Spectrochim. Acta.* 31A:1729–1737.

Talluri, S., D. M. Rothwarf, and H. A. Scheraga. 1994. Structural characterization of a three-disulfide intermediate of ribonuclease A involved in both the folding and unfolding pathways. *Biochemistry.* 33: 10437–10449.

Thompson, P. A., W. A. Eaton, and J. Hofrichter. 1997. Laser temperature jump study of the helix⇄coil kinetics of an alanine peptide interpreted with a 'kinetic zipper' model. *Biochemistry.* 36:9200–9210.

Tsong, T. Y., R. P. Hearn, D. P. Wrathall, and J. M. Sturtevant. 1970. A calorimetric study of thermally induced conformational transitions of ribonuclease A and certain of its derivatives. *Biochemistry.* 9:2666–2677.

Tsuji, Y., T. Yasunaga, T. Sano, and H. Ushio. 1976. Kinetic studies of the helix-coil transition in aqueous solutions of poly(alpha-L-glutamic acid) using the electric field pulse method. *J. Am. Chem. Soc.* 98:813–818.

Wada, A., T. Tanaka, and H. Kihara. 1972. Dielectric dispersion of the α-helix at the transition region to random coil. *Biopolymers.* 11: 587–605.

Wearne, S. J., and T. E. Creighton. 1988. Further experimental studies of the disulfide folding transition of ribonuclease A. *Proteins.* 4:251–261.

Williams, A. P., C. E. Longfellow, S. M. Freier, R. Kierzek, and D. H. Turner. 1989. Laser temperature-jump, spectroscopic, and thermodynamic study of salt effects on duplex formation by dGCATGC. *Biochemistry.* 28:4283–4291.

Williams, S., T. P. Causgrove, R. Gilmanshin, K. S. Fang, R. H. Callender, W. H. Woodruff, and R. B. Dyer. 1996. Fast events in protein folding: helix melting and formation in a small peptide. *Biochemistry.* 35: 691–697.

Yamamoto, K., Y. Mizutani, and T. Kitagawa. 1999. Time-resolved Raman spectra of protein solutions observed with a novel nanosecond temperature jump apparatus. 9th Intl. Conf. Time-Resolved Vibrational Spectroscopy, Tucson, Arizona, P12-A.